# TECHNICAL REPORT

## EXPERIMENTAL STUDIES OF LOW-DENSITY EFFECTS IN HYPERSONIC WEDGE FLOWS

By: R.J. Vidal and J.A. Bartz

## CAL No. AF 1500-A-2

Prepared For:

Air Force Office of Scientific Research
Office of Aerospace Research
United States Air Force
Washington, D.C. 20333

Contract No. AF 49(638)-952
December 1964

CORNELL AERONAUTICAL LABORATORY, INC.
OF CORNELL UNIVERSITY, BUFFALO, N. Y. 14221

AFOSR 65-0335

CORNELL AERONAUTICAL LABORATORY, INC.
BUFFALO, NEW YORK 14221

REPORT NO. AF 1500-A-2

# EXPERIMENTAL STUDIES OF LOW-DENSITY EFFECTS IN HYPERSONIC WEDGE FLOWS

CONTRACT NO. AF 49(638)-952



PREPARED FOR
MECHANICS DIVISION
AIR FORCE OFFICE OF SCIENTIFIC RESEARCH
OFFICE OF AEROSPACE RESEARCH
WASHINGTON, D.C. 20333

BY: R. J. Vidal
R.J. Vidal

J.A. Bartz
J.A. Bartz

APPROVED:
A. Hertzberg, Head
Aerodynamic Research Department

## FOREWORD

The research described in this report was sponsored by the U.S. Air Force through the Office of Scientific Research, Contract AF 49(638)-952. The technical monitor was Milton Rogers, Chief, Mechanics Division, AFOSR. A paper on this research was presented at the Fourth International Symposium on Rarefied Gas Dynamics, Toronto, Canada, 14-17 July, 1964.

The authors gratefully acknowledge the many stimulating discussions during the course of this research with Dr. J.G. Hall and Dr. H.K. Cheng of the Aerodynamic Research Department.

## ABSTRACT

Experimental heat transfer and pressure data are presented which extend from the classical thin boundary layer regime to near-free-molecule flow (Knudsen numbers based on ambient stream conditions as large as 5). These data are compared with viscous shock layer theory for heat transfer and with theory for the combined effects of wedge angle and boundary layer displacement to define the theoretical range of validity and to identify the low density departures from boundary layer theory. It is noted that low density effects are first evident in the pressure data. It is concluded that the cause of these departures cannot be identified within existing solutions based on the Navier-Stokes relations. It is hypothesized that the departures might stem from second-order (Burnett) molecular effects.

TABLE OF CONTENTS

## LIST OF ILLUSTRATIONS

## NOMENCLATURE

| | |
|---|---|
| $a_e$ | thermal accommodation coefficient |
| $C_*$ | modified Chapman-Rubesin constant, $\frac{\mu(T_*)}{\mu_\infty}\ \frac{T_\infty}{T_*}$ |
| $C_H$ | Stanton number |
| $H$ | total enthalpy |
| $M$ | free stream Mach number |
| $p$ | hydrostatic pressure |
| $q$ | heat flux per unit area |
| $Re_x$ | Reynolds number, $\frac{\rho_\infty U_\infty x}{\mu_\infty}$ |
| $T$ | temperature |
| $T_*$ | modified reference temperature, $\frac{T_*}{T_o} = \frac{T_w}{T_o} + \frac{1}{2}\left(1 - \frac{T_w}{T_o}\right) - \frac{1}{3}\cos^2\alpha$ |
| $U_\infty$ | free stream velocity |
| $u, v$ | velocity components in $x$ and $y$-direction, respectively |
| $x$ | distance along x edge, measured from the leading edge |
| $y$ | distance measured normal to wedge surface |
| $\alpha$ | wedge semiangle |
| $\gamma$ | ratio of specific heats |
| $\theta$ | shock angle |
| $\lambda$ | molecular mean free path |
| $\mu$ | viscosity |
| $\rho$ | density |
| $\sigma_y$ | normal stress in gas adjacent to surface |
| $\bar{\iota}$ | $= M^3 \sqrt{\frac{C_*}{Re_x}}$ |
| $\bar{\iota}_\epsilon$ | $= \frac{\gamma-1}{\gamma+1}\left(0.664 + 1.73\frac{T_w}{T_o}\right) M^3 \sqrt{\frac{C_*}{Re_x}}$ |

Subscripts

| | |
|---|---|
| $\infty$ | free stream condition |
| G | gas condition |
| W | wall condition |
| O | reservoir condition |

# 1. INTRODUCTION

A fundamental problem in rarefied gas flows over bodies is to describe the transition between the continuum situation and the free-molecule limit. One basic difficulty is that the governing relations for the flow have not been established. The Navier-Stokes relations, as derived from a continuum viewpoint, have been duplicated with kinetic theory as a first-order approximation in molecular mean free path. Second-order approximations in molecular mean free path have been derived by Burnett[1] and by Grad,[2] but since there is no established continuum equivalent for these relations, the physical significance of the second-order terms is not clear. Consequently, the main effort has been to use the first-order (Navier-Stokes) approximation as the governing relations and to account for the fluid processes induced by the body that are consistent with these relations. The resulting solutions then require experimental checks to determine their range of validity and to indicate where the next order of approximation might be required.

The purpose of this paper is to present heat transfer and pressure data obtained with two-dimensional wedge models (sharp leading edges) in the CAL Six-Foot Hypersonic Shock Tunnel. These data virtually span the entire transition regime, extending from the classical thin boundary-layer regime to Knudsen numbers (based on ambient stream conditions) as large as 5. The intent here is to test the available theories dealing with wedges in a continuum flow in order to define their limits of validity, and to provide data in the transition regime. These wedge models are particularly useful in this transition regime for several reasons. First, the two-dimensional models,

as compared with three-dimensional models, make it feasible to incorporate instrumentation closer to the leading edge and hence more closely approach the free-molecule limit. Second, the simple wedge configuration tends to suppress a variety of low-density fluid processes associated with blunt bodies that complicate the data interpretation. Third, by varying the wedge angle, it is possible to change the dominant low-density mechanism governing the initial departures from the continuum regime.

In the succeeding sections, the basis for the applicable theories will be briefly reviewed in order to indicate those items that could influence the observed low density departures. Following this, the experimental apparatus will be briefly described, leading to the presentation and discussion of the experimental data.

## II. WEDGE THEORIES

### A. Boundary-Layer Displacement Theory

The problem of hypersonic viscous flow over a wedge has been considered for over a decade, and pioneering theoretical research was accomplished by Shen,[3] Pai,[4] and by Pai and Shen.[5] More recently Cheng et al.[6] have presented a unified approach to this and related boundary layer problems which has a wide range of applicability. Cheng's theory for the thin boundary layer regime will be used for comparison with the data in the present paper.

Briefly, the basis for Cheng's theory is in the Navier-Stokes approximation which is specialized, for the case of large Mach numbers and small disturbances, to the boundary layer equations. Using the appropriate similarity transformation, these are reduced further to the Blasius equations for the case of $\frac{\gamma-1}{\gamma+1} \ll 1$ and/or a sufficiently small axial pressure gradient.

In this way it is shown that if the shock layer is not fully viscous and if slip at the surface is negligible, there is a similarity between the transformed velocity profile, $\frac{u}{U_\infty}$, and the transformed enthalpy profile, $\frac{H - H_\infty}{H_w - H_\infty}$.

There are several important conclusions to be noted in connection with this theory. First, because of the similarity in the governing tangential momentum and energy equations, it is possible to immediately write a general relation between the heat transfer to the surface and the local hydrostatic pressure.

$$M^3 C_H \equiv \frac{M^3 q}{\rho_\infty U_\infty (H_\infty - H_w)} = 0.332 M^3 \sqrt{\frac{C_*}{Re_L}} \frac{p/p_\infty}{\sqrt{\int_0^x \frac{p}{p_\infty} \frac{dx}{L}}} \qquad (1)$$

The details of this computation can be obtained from the original paper.[6] One implication in this result is that the heat transfer to the surface and the hydrostatic pressure at the surface are simply related. Within the framework of this theory, low density departures from the theory should be observed simultaneously in both the heat transfer and the hydrostatic pressure at the surface.

The second important conclusion reached in this wedge theory is that the hydrostatic pressure on the compression side of the wedge is accurately given by the sum of the inviscid wedge pressure and the induced pressure due to boundary layer displacement. This leads to the following expression, consistent with the approximations used by Cheng.

$$\frac{p}{p_\infty} \approx \gamma M^2 \alpha^2 + \frac{\sqrt{3}}{2} \gamma \bar{t}_\epsilon$$

$$\bar{t}_\epsilon = \frac{\gamma - 1}{\gamma + 1} \left(0.664 + 1.73 \frac{T_w}{T_0}\right) M^3 \sqrt{\frac{C_*}{Re_x}}$$

The form used in the present work includes a more accurate expression for the pressure behind an oblique shock wave.

$$\frac{p}{p_\infty} \approx \frac{2\gamma}{\gamma+1} M^2 \sin^2\theta + \frac{\sqrt{3}}{2} \gamma \bar{\epsilon}_\epsilon \tag{2}$$

Substituting in Eq. 1 leads to the following expression for the surface heat transfer,

$$M^3 C_H = 0.166(3)^{1/4} \bar{\epsilon}_\epsilon \sqrt{\gamma \bar{\epsilon}_\epsilon} \frac{\left[1 + \frac{4}{\sqrt{3}(\gamma+1)} \frac{M^2 \sin^2\theta}{\bar{\epsilon}_\epsilon}\right]}{\left[1 + \frac{2}{\sqrt{3}(\gamma+1)} \frac{M^2 \sin^2\theta}{\bar{\epsilon}_\epsilon}\right]^{1/2}} \tag{3}$$

where $\theta$ is the shock wave angle and is related to the wedge angle, $\alpha$, through the oblique shock wave relations.

The third important item to be noted in connection with Cheng's theory concerns the range of validity for the theory. The model used should remain valid, within the Navier-Stokes approximation, as long as there is an essentially inviscid region behind the shock wave, and as long as the slip velocity and energy jump at the surface are small. The latter requires that the molecular mean free path be small at the surface.

Cheng's theory for the combined effects of wedge angle and boundary layer displacement has been experimentally checked, within its range of validity, as a part of comprehensive experimental research on heat transfer to sharp and blunted flat plates by Hall and Golian.[6,7] Pressure data obtained by Hall and Golian also confirmed the theory at zero wedge angle.

B. Viscous Shock-Layer Theory

More recently Cheng has extended his work on the wedge problem to allow for a fully viscous shock layer.[8] This work, which is one part of a

comprehensive treatment of the blunt-body problem, takes account of the transport effects, as they alter the boundary conditions at the shock wave. The development is based on the Navier-Stokes equations which are specialized to the viscous shock-layer equations. These differ from the boundary layer equations in that the normal and tangential pressure gradient terms are retained.

The details of this viscous shock-layer formulation can be obtained from the original paper.[8] Several points are of importance to the present work. First, the viscous shock layer problem is fundamentally nonsimilar since the boundary conditions to be satisfied at the shock wave are non-similar. The solutions given by Cheng were obtained using machine methods. These are restricted to large wedge semiangles (greater than about 20° but smaller than the shock wave detachment angle of about 42 1/2°). This restriction to large angles makes it possible to neglect viscous layer displacement effects and surface-slip effects. With these restrictions and within the Navier-Stokes model, the surface pressure is simply the hydrostatic pressure behind the oblique shock wave. The skin friction and heat transfer to the surface are less than the Blasius prediction since the transport effects at the shock wave convect away energy and tangential momentum.

The numerical solutions given by Cheng yield the Blasius solution in the limit of high Reynolds numbers. In addition, they yield the free-molecule limits for the case of vanishing Reynolds number. This low-Reynolds number behavior evidently is due to the proper conservation of energy and momentum through the modified boundary conditions at the shock wave.

## III. EXPERIMENTAL APPARATUS AND TEST CONDITIONS

### A. Apparatus

#### 1. Tunnels

The low-density investigations were made in the CAL Six-Foot Hypersonic Shock Tunnel shown in Fig. 1. In addition, certain high-density, low Mach number experiments were made in the CAL 48" Hypersonic Shock Tunnel to completely span the transition between the classical thin boundary layer regime and the strong interaction regime. These facilities have been discussed in connection with earlier low density research,[9] describing the available range of test conditions, the mode of operation, the test section calibrations, the effects of nozzle thermochemical nonequilibrium, and the calculation of ambient test section conditions.

#### 2. Flow Angularity

It was noted earlier[9] that there was some uncertainty concerning the flow angularity in the tunnel test section which could influence the low density data. Since that work, detailed angularity calibrations have been made using the small flat-plate model described below. This calibration exploits the extreme sensitivity of flat plate heat transfer to small wedge angles under near-free molecule conditions. Typically, a one degree change in angle produces a 70% change in heat transfer. The flat plate heat transfer was measured over a range of positive and negative angles in order to determine the change in heat transfer with wedge angle and to determine the wedge angle where the heat transfer was independent of model rotation in the tunnel. These experiments showed the flow angularity was about 0.1° with an experimental uncertainty of $\pm 0.1°$. Consequently, it is concluded that the effects of flow angularity

are negligible in these experiments.

### 3. Models

Two flat-plate models were used in the experimental wedge research (Fig. 2). The wedge flows were produced by pitching the models to various compression angles. The small-scale model, designed to investigate the leading-edge region, consisted of fourteen thin-film (platinum) thermometers mounted on a Pyrex glass plate. This glass plate was bonded to a steel plate. Typically, these thermometers were 0.02" x 0.25" and near the leading edge were spaced about 0.02" apart. All fourteen gages were located within about 1" from the leading edge, and under typical test conditions, five gages were within one ambient mean free path from the leading edge. The first gage was at the leading edge. The gage wire lead was gold film about 2 microns thick, leading to a conventional wire lead at the model extremities. The entire model was coated with titanium dioxide about 0.1 microns thick to prevent electrical shorting in ionized flows. The operating principles of the thin-film gage as well as the coated gage have been described in the literature.[10-12] and will not be reviewed here.

The leading edge of the small-scale model was flat-faced with a thickness estimated to be 0.005". The wedge angle of the lower surface was 30°. During experiments at small wedge angles, it was found that the first gage indicated a heat transfer rate about twice that at the next station. It has been determined that this behavior was due to heat conduction from the blunt leading edge and the lower surface. Under free-molecule conditions, the heat transfer rates to the blunt leading edge and to the wedge lower surface are respectively sixty times and thirty times greater than that to the upper surface. Heat

conduction calculations showed that this would cause a 100% change in indicated heat transfer to the instrumented surface. Experiments were made with the instrumented surface shielded from the flow to measure the heating from both surfaces. These tests verified the above calculation. The data that were affected by this additional heating are not reported.

The large-scale flat plate model shown in Fig. 2 consisted of a steel plate with detachable leading and trailing edges. The model instrumentation included platinum thin-film resistance thermometers and piezoelectric pressure transducers. The model leading edge was a 30° wedge honed to a thickness of the order of $5 \times 10^{-4}$ inches. A complete description of this model, including chordwise and spanwise effects, lag time associated with pressure orifice size, and model support, is given in Ref. 9. The effects due to a finite span and a finite chord were examined in the present research and found to be negligible except for wedge semiangles larger than 45°. The effects of a finite chord for these conditions will be discussed in the next section.

B. Low-Density Orifice Effects

The usual approach in interpreting pressure measurements is to assume the measured pressure is the local hydrostatic pressure at the surface. This is a valid assumption if the molecular mean free path at the surface is much smaller than the orifice diameter and/or the gas and surface are in thermal equilibrium. However, if the molecular mean free path is comparable to or greater than the orifice diameter and if the surface temperature differs from the gas temperature, a thermal transpiration effect is encountered. This effect can be explained by considering the limit where the mean free path is much larger than the orifice. Under such conditions, assuming no gradients in the gas, mass continuity

requires that

$$\rho_w \sqrt{T_w} = \rho_G \sqrt{T_G}$$
$$\frac{p_w}{p_G} = \sqrt{\frac{T_w}{T_G}} \tag{4}$$

where the subscripts $w$ and $G$ refer to surface and gas conditions, respectively.

The above transpiration formulas apply only if the orifice diameter is much smaller than the molecular mean free path. In the present experiments the orifice diameter was comparable to the mean free path, and the measured pressure was corrected by using an empirical formula given by Knudsen.[13] Knudsen conducted a series of transpiration experiments with hydrogen in heated tubes in which the ratio of the tube diameter to the molecular mean free path was varied over a wide range. He found that all data correlated within about 4% with the formula

$$\frac{p_w}{p_G} = \left(\frac{T_w}{T_G}\right)^{\frac{1}{2K(\lambda)}}$$
$$K(\lambda) = \left[1 + 1.23 \frac{d}{\lambda_w}\left(\frac{1+1.575 \frac{d}{\lambda_w}}{1+12.25 \frac{d}{\lambda_w}}\right)\right]^2 \tag{5}$$

where $d$ is the orifice diameter and $\lambda_w$ is the molecular mean free path at the wall conditions. Knudsen's original experiments have been duplicated by Arney and Bailey[14,15] for air, argon, and helium, and have verified Knudsen's empirical formula with errors of less than 5%.

The pressure data from the present experiment have been corrected using Knudsen's formula, Eq. 5, and the gas temperature as calculated from the measured heat transfer rate. It can be shown, consistent with the Navier-Stokes

approximation,[16] that the gas temperature near a surface is

$$T_G = T_w + \frac{75\pi}{128}\,\lambda_G\,\frac{\partial T}{\partial y} + \frac{(\gamma-1)\,u_G^2}{4\gamma\,C_p} \tag{6}$$

where $C_p$ is the specific heat at constant pressure. Within this approximation, the heat transfer to the surface is

$$q = -k_G\,\frac{\partial T}{\partial y} - \mu_G u_G\,\frac{\partial u}{\partial y} \tag{7}$$

The gas temperature expressed in terms of the heat transfer rate is

$$C_p T_G = C_p T_w + \frac{75\pi}{128}\left(\frac{\lambda C_p}{k}\right)_G q + \frac{u_G^2}{4}\left(\frac{\gamma}{(\gamma-1)} - \frac{15}{2}\,Pr\right) \tag{8}$$

The magnitude of the velocity terms in Eq. 8 has been estimated for the thin boundary layer regime, using Cheng's theory[6] and was found to be less than 10% over the density range of interest. Consequently, they were neglected and the gas temperature was taken as

$$\left(\frac{T_G}{T_w}\right)^{1/2} = \frac{15}{8}\sqrt{\frac{\pi(\gamma-1)}{2\gamma}}\,\frac{Pr\,q}{\gamma C_p T_w}\,\frac{1}{p_G} \tag{9}$$

Equations 5 and 9 were combined to obtain a relation for the ratio of the measured pressure to the gas pressure in terms of measured heat transfer rate and pressure which was used to correct for the orifice effects. The correction amounted to about 50% at the lowest density and a few percent at the highest density.

There are two important assumptions inherent in this correction. First, Knudsen's experiments were made with long circular tubes, while the present data were obtained using relatively short tubes with approximately elliptical cross sections (length-to-width ratio of 2). The effective diameter was taken to be the hydraulic diameter. The second approximation is the neglect of the gradients in the gas. Knudsen's experiments were made with

tubes connecting constant temperature reservoirs, while in the present experiments the gas was markedly nonuniform. These two items introduce some doubt as to the relevance of Knudsen's tube correction for the orifice effect in the present data.

The applicability of Knudsen's semi-empirical tube formula to the orifice effect has been checked with direct measurements of surface pressure. One of the piezoelectric pressure transducers used in orifice measurements was modified so that the 1/2-inch diaphragm was flush with the surface.* This instrument was mounted in the large-scale flat plate model, five inches from the leading edge and adjacent to an orifice transducer. The model was then tested at low density conditions where orifice measurements indicated the chordwise variations in surface pressure were negligible (15% over an eight inch length). The pressures measured by the adjacent orifice and surface pressure transducer differed by a factor of 1.64, as compared with a factor of 1.60 predicted with Knudsen's formula. Consequently, it is concluded that the present data, corrected with Knudsen's formula, can be interpreted as the surface pressure.

## IV. EXPERIMENTAL RESULTS

In the subsequent discussion, the experimental data will be presented and compared with the wedge theories described in Section II. The comparison first will be made with the viscous shock layer theory to demonstrate its accuracy and to explore its range of validity. Included are previously-reported data obtained at zero-angle of attack and at large wedge angles.[9,17]

---

*The flush-diaphragm transducer was developed earlier at CAL by Mr. R. MacArthur of the Applied Hypersonic Tunnel Department.

A. Viscous Shock Layer Regime

The heat transfer data obtained with wedge semiangles of 2°, 5°, 10°. 20°, 30°, 40°, 45°, 60°, and 75° are compared with the viscous shock layer theory[8] in Fig. 3. Consider first the data obtained at wedge semiangles of 20°, 30°, and 40°, where the theory is expected to be valid. It can be seen that the data are in good agreement with the theory over the entire density range. The data tend to fall about 15% above the theory even in the high Reynolds number (Blasius) limit ( $\frac{Re_x}{\gamma M^2 C_* \cos\alpha} > 1.0$), and approach the free-molecule limit at small Reynolds numbers. As the wedge semiangle is decreased ( $\alpha$ = 10°, 5°, 2°), the data tend to fall progressively above the theory in the high Reynolds number limit, but tend to approach the correct free-molecule limit for a unit accommodation coefficient. It is believed that this behavior at high densities can be ascribed to viscous layer displacement effects which are neglected in the theory. That is, the theory assumes that the rate of growth of the viscous layer is negligible in comparison with the wedge semiangle. As a check on this displacement effect, the theory for the combined effects of wedge angle and boundary layer displacement[6] has been used to estimate the heat transfer. The relation given in Eq. 3 was used here. It can be seen that the data tend towards that estimate in the high Reynolds number limit, indicating the departures from the theory are, in part, due to displacement effects. The displacement theory for $\alpha$ = 20°, 30°, and 40° is essentially independent of wedge angle when plotted in terms of the parameters in Fig. 3. The estimate of the displacement effects is in good agreement with the data in the high Reynolds number limit. Consequently, it is concluded that the 15% discrepancy between viscous-layer theory and

experiments observed within the theoretical range of validity is largely due to viscous layer displacement effects. The departures at small wedge angles stem, at least in part, from the neglected displacement effects.

There is one further item to be noted in Fig. 3 in the comparison between displacement theory and experiment at small wedge angles. At $\alpha$ = 20°, 30°, and 40°, the low density effects first become apparent at $\frac{Re_x}{\gamma M^2 C_* \cos\alpha} \lesssim 0.5$. In contrast, at $\alpha$ = 2°, the low density effects become apparent at $\frac{Re_x}{\gamma M^2 C_* \cos\alpha} \lesssim 5.0$. One mechanism neglected in both the viscous shock layer theory and the displacement theory is slip at the surface. It can be demonstrated that the ratio of the shock wave transport effect to the surface slip effect varies approximately as the ratio of the molecular mean free path at the shock wave to that at the surface. This ratio has been calculated using the oblique shock wave relations and is tabulated in Fig. 3. It can be seen that for $\alpha$ = 20°, 30°, and 40°, the ratio of the mean free paths is $3\ 1/2 < \frac{\lambda_s}{\lambda_w} < 12$ indicating that the shock wave transport effect is dominant for these wedge angles. However, for $\alpha \leq 10°$, the ratio of mean free paths is $\frac{\lambda_s}{\lambda_w} \leq 1.3$, indicating that slip effects at the surface are at least comparable in magnitude to the shock wave transport effects. In fact, at $\alpha$ = 2° the surface slip effects should be at least 3 to 4 times greater than the transport effects.

Before leaving the data obtained at small wedge angles, it should be noted that an approximate criterion can be derived for the lower limit of validity, in wedge semiangle, for the viscous shock layer theory. The data and the comparisons with theory in Fig. 3 suggest that displacement effects are the major cause of the departures from the viscous shock layer theory.

These departures are greatest at $\frac{Re_x}{\gamma M^2 C_* \cos\alpha} \approx 1.0$. The displacement effects have been calculated at this value of the rarefaction parameter; they amount to 13% and 24% at $\alpha = 20°$ and 15° respectively. On this basis it is concluded that the viscous shock layer theory is accurate for wedge semiangles as small as 20°.

It was noted in Section II that the viscous shock layer theory for wedge flows should be valid only if the shock wave is attached. This corresponds to a maximum wedge angle of $\alpha \approx 42\ 1/2°$ for $M \longrightarrow \infty$. The accuracy of this theory for detached shock waves was investigated with experiments at $\alpha = 45°$, 60°, and 75°, Fig. 3. It can be seen that the theory is generally quite accurate, underestimating the heat transfer by about 30% in the high Reynolds number limit. The data at low Reynolds numbers approach the free-molecule limit and agree quite well with the theory. One item to be noted is the distinct trailing edge effect in these data. For example, note the data obtained with the large model and the small model at $\alpha = 75°$. Those obtained near the trailing edge of the small model fall about 50% above the data from the center of the large model.

B. Boundary-Layer Displacement Effects

It was noted in the discussion of Fig. 3 that displacement effects are important at small wedge angles. Since the viscous shock layer theory for large wedge angles predicts that the hydrostatic pressure at the surface should be that for an inviscid wedge, it is pertinent to compare all data with the theory for the combined effects of wedge angle and boundary layer displacement.[6]

These comparisons, Figs. 4 and 5, include data for $\alpha = 0$ which were previously reported.[9] They have been included in these comparisons by

assuming an arbitrarily small wedge angle ( $\alpha = 10^{-2}$ rad.). That is, the governing parameters for the combined wedge angle-displacement theory were evaluated at $10^{-2}$ radians where wedge effects are negligibly small. The corresponding free-molecule limit was evaluated at the same wedge angle. The heat transfer data, Fig. 4, are in good agreement with the theory near the trailing edge (large values of $\frac{M^2 \sin^2 \theta}{\bar{\tau}_G}$ ), and the low density effects appear as the data fall below the theory near the leading edge. The data obtained at large wedge angles ( $\alpha = 20°, 30°, 40°$) are seen to agree well with the wedge limit, and the displacement effects discussed earlier are apparent in this presentation. It should be noted that all data approach the appropriate free-molecule limit (unit accommodation coefficient). The interesting item here is that the data obtained at all finite wedge angles approach the free-molecule limits without overshoot. In contrast, the $\alpha = 0°$ data initially overshoot the free-molecule limit and approach it from above.

The corrected pressure data are compared with the theory for displacement and wedge effects in Fig. 5. Consider first the data obtained at large wedge angles ( $\alpha = 20°, 30°, 40°$). It can be seen that these data are in reasonable agreement with the wedge limit ( $\frac{1}{\gamma M^2 \sin^2 \theta} \frac{p}{p_\infty} \approx 1.0$), falling somewhat higher than this limit. This can be ascribed to the approximate relation used for pressure in the theory for the wedge limit. The theory predicts a significant boundary layer displacement effect for $\alpha = 20°$, while the data fall somewhat below this estimate. As the wedge angle is decreased further to 2°, the data depart further from the theory, differing by a factor of 3 to 4 at $\alpha = 2°$. However, the high density data for $\alpha = 0°$ agree well

with the theory. Consequently, it must be concluded that the theory is basically correct, and that these departures stem from a low density effect not included in the theory.

These departures and those observed in the heat transfer are summarized in Table I. This tabulation lists the value of $\frac{M^2 \sin^2 \theta}{\bar{\imath}_e}$ where the heat transfer first departs from the theory, and the magnitude of the departures in pressure at that value of the governing parameter.

TABLE I

Discrepancy Between Theory and Experiment for Surface Pressure and Heat Transfer

| Wedge Semiangle | $\frac{M^2 \sin^2 \theta}{\bar{\imath}_e}$ | $\frac{C_{H_T} - C_{H_{exp}}}{C_{H_T}}$ | $\frac{(p/p_\infty)_T - (p/p_\infty)_{exp}}{(p/p_\infty)_T}$ |
|---|---|---|---|
| 40° | 2.0 | 0% | 0% |
| 30° | 1.2 | 0% | 28% |
| 20° | 0.7 | 0% | 35% |
| 10° | 0.2 | 0% | 60% |
| 5° | 0.12 | 0% | 64% |
| 2° | 0.03 | 0% | 69% |

It can be seen both in Fig. 4 and 5 and in Table I that there is virtually no agreement in the point where low density departures are first observed in the heat transfer and in the pressure. This behavior is surprising in view of the comments made in Section II. The theory is based upon similarity between the enthalpy and velocity profiles in the boundary layer. This similarity makes it possible to cast the expression for the heat transfer in terms of the hydrostatic pressure. From this relation it might be

expected that the departures of heat transfer from theory would vary as the square root of the hydrostatic pressure. The data do not confirm this expectation. Further, this behavior does not seem to be associated with the shock layer becoming fully viscous since the effect is apparent in the $\alpha = 20°$ data. The data for $\alpha = 20°$ fall in the range of validity for the viscous shock layer theory, which predicts that the surface pressure is the hydrostatic pressure for the inviscid wedge. The observed effect might stem from the shock wave thickening or from a normal pressure gradient. Cheng[8] has shown that in the viscous shock layer regime for wedges, the shock thickening effect and the normal pressure gradient are of higher order than the transport effects at the shock wave. More recently Probstein and Pan[18] have considered these effects in an analysis of the sharp flat plate at zero angle of attack using the Navier-Stokes approximation. They show that these effects, combined with first-order surface slip and shock wave transport effects, only produce a 25% departure from displacement theory. Finally, this behavior might be ascribed to a breakdown in the strong shock wave approximation, the limiting density ratio approximation, or the small disturbance approximation. However, if this were the case, the heat transfer should reflect this breakdown since the heat transfer is determined by the pressure distribution. It appears that the observed departures cannot be explained within the framework of existing Navier-Stokes analyses.

C. Additional Molecular Effects

The main feature apparent in the experimental data is that the low-density effects are first evident in the measured pressure. The pressure departs markedly from boundary layer theory in a range of the rarefaction

parameter, $\frac{M^2 \sin^2\theta}{\bar{\gamma}_\epsilon}$, where the heat transfer data are in good agreement with the same theory. This behavior could stem from several sources.

One possible cause of the observed behavior is in the interpretation of pressure. Boundary layer theory takes the surface pressure to be the local hydrostatic pressure in the gas; that is, the average value of the three normal stresses in the gas. The correct gas pressure is the stress in the gas normal to the surface. Within the Navier-Stokes approximation, this normal stress, in two dimensions, is

$$\frac{\sigma_y}{p} = 1 + \frac{2}{3}\frac{\mu}{p}\left(\frac{\partial u}{\partial x} - 2\frac{\partial v}{\partial y}\right) \tag{10}$$

where $\sigma_y$ is the normal stress adjacent to the surface. It can be seen that if the slip velocity at the surface is appreciable, the normal stress could differ from the hydrostatic pressure. The magnitude of the normal stress at the surface has been estimated using the theory of Ref. 6. The calculation shows the normal stress at the surface to be

$$\frac{\sigma_y}{p} = 1 - \frac{f_{\eta\eta}\sqrt{\pi}}{4(3)^{3/4}\delta^3}\left\{\frac{(\gamma-1)\frac{\bar{\gamma}_\epsilon}{M^2}\frac{T_w}{T_o}}{1+\frac{2}{\sqrt{3}(\gamma+1)}\frac{M^2\sin^2\theta}{\bar{\gamma}_\epsilon}}\right\}^{3/2}\left\{1+\frac{4}{3}\frac{\left[1+\frac{2}{\sqrt{3}(\gamma+1)}\frac{M^2\sin^2\theta}{\bar{\gamma}_\epsilon}\right]}{\left[1+\frac{4}{\sqrt{3}(\gamma+1)}\frac{M^2\sin^2\theta}{\bar{\gamma}_\epsilon}\right]^2}\right\} \tag{11}$$

where $f_{\eta\eta}$ is the slope of the Blasius profile at the surface and

$$\delta = \frac{\gamma-1}{\gamma+1}\left(0.664 + 1.73\frac{T_w}{T_o}\right)$$

For the cold-wall conditions of the present experiments, Eq. 7 is approximately

$$\frac{\sigma_y}{p} \approx 1 - \frac{1}{40}\left\{\frac{\frac{\bar{\ell}_\epsilon}{M^2}}{1+\frac{2}{\sqrt{3}(\gamma+1)}\frac{M^2\sin^2\theta}{\bar{\ell}_\epsilon}}\right\}^{3/2}\left\{1+\frac{4}{3}\frac{\left[1+\frac{2}{\sqrt{3}(\gamma+1)}\frac{M^2\sin^2\theta}{\bar{\ell}_\epsilon}\right]}{\left[1+\frac{4}{\sqrt{3}(\gamma+1)}\frac{M^2\sin^2\theta}{\bar{\ell}_\epsilon}\right]^2}\right\} \quad (12)$$

To illustrate, consider Eq. 12 in the limit of dominant displacement effects (vanishing $M^2\sin^2\theta$). This limit corresponds to the largest low-density effects, and the first departures from boundary layer theory are observed at $\frac{\bar{\ell}_\epsilon}{M^2} \approx 2 \times 10^{-2}$. It can be seen that, within the Navier-Stokes approximation, the normal stress differs from the hydrostatic pressure by less than 0.1%. Consequently, it is concluded that, within the Navier-Stokes approximation, this difference is not the cause of the observed effects.

A second possible source of the observed departures in the pressure is in the transpiration correction applied to the data. It was noted in Section III B that the correction was based upon Knudsen's experiments involving pseudo transpiration between constant-temperature reservoirs. In contrast, the present experiments involved pseudo transpiration with large gradients in the gas. The effects of these gradients on the pressure correction can be estimated, within the Navier-Stokes relations, by considering the transpiration effect for a nonuniform gas. The basis for this computation can be obtained from Ref. 16 using the continuity requirement in the calculation of the slip boundary conditions. Neglecting the details of the calculation, it can be shown that, for an orifice diameter much smaller than the mean free path in the gas, the ratio of the measured pressure to the hydrostatic pressure in the gas in two dimensions is

$$\frac{p_w}{p_e} = \sqrt{\frac{T_w}{T_e}} \left[ 1 + \frac{1}{3} \frac{\mu}{p} \left( \frac{\partial u}{\partial x} - 2 \frac{\partial v}{\partial y} \right) \right] \qquad (13)$$

Comparing Eq. 13 with Eqs. 4 and 10, it can be seen that the correction term for the gradients in the gas is simply half of the correction term for the normal stress in the gas. Consequently, it is concluded that, within the Navier-Stokes approximation, the gradients have a negligible effect on the transpiration correction.

A third possible source of the observed departures in the pressure is second-order molecular effects. This possibility was first noted by Maxwell[19] in 1879 in his paper, "On Stresses in Rarefied Gases Arising from Inequalities in Temperature". In particular, Maxwell retained certain second-order terms in a formal kinetic-theory development of the (first-order) Navier-Stokes relations to show that additional temperature terms appeared in the stress tensor. This second-order theory was subsequently completed by Burnett[1] and by Grad,[2] retaining all second-order terms. If the second-order stress tensor is examined, it is found that the normal stress in the gas varies as

$$\frac{\partial_y}{p} = 1 + \frac{2}{3} \frac{\mu}{p} \left( \frac{\partial u}{\partial x} - 2 \frac{\partial v}{\partial y} \right) + \left( \frac{\mu}{p} \right)^2 \left[ C_1 \left( \frac{\partial T}{\partial y} \right)^2 + C_2 \frac{\partial^2 T}{\partial y^2} + \cdots \right] \qquad (14)$$

where $C_1$ and $C_2$ are known constants. It was shown earlier that the first-order term in the normal stress is negligibly small for the cold wall conditions of the present experiments. The second-order terms can be large, however, owing to the high stagnation temperature and the low wall temperature. To illustrate, the temperature gradient near the wall in the present experiments

is of the order of $5 \times 10^4$°K/ft., which is large enough to make the second-order terms appreciable (10-30%). It is clear that second-order molecular effects cannot be neglected a priori, and that the observed departures between theory and experiment could indicate that the Navier-Stokes relations are inapplicable.

## V. CONCLUDING REMARKS

Experimental heat transfer and pressure data obtained with wedge models in a hypersonic shock tunnel have been presented and compared with boundary layer theory and with viscous shock layer theory. These data, which virtually span the entire transition from continuum to near-free-molecule flows, show that the viscous shock layer theory for heat transfer is in error by less than 15% in the theoretical range of validity (wedge semiangles greater than 20° but less than that for shock wave detachment). The heat transfer data obtained with a detached shock wave show that the theory can be used to estimate heat transfer under these conditions with an error of less than 25% if the wedge trailing edge is sufficiently far downstream. For wedge half-angles of less than 20°, the data show that the viscous shock layer theory for heat transfer progressively breaks down with decreasing wedge angle. Comparisons with boundary layer theory in the high Reynolds number limit indicate the breakdown in the viscous shock layer theory is largely due to the neglect of the viscous layer thickness in comparison with the wedge thickness.

A comparison of the heat transfer data with boundary layer theory for the combined effects of wedge angle and boundary layer displacement show that the data are in good agreement with the theory in the high Reynolds number limit. The data depart near the leading edge and, for all wedge semiangles

e ual to or greater than 2°, approach the free-molecule limit from below that limit. In contrast, the pressure data agree with the theory only at much larger Reynolds numbers. The discrepancies between theory and experiment at equal values of the rarefaction parameter are much larger for pressure than for heat transfer, and the cause of this behavior cannot be identified within existing solutions based upon the Navier-Stokes approximation. Cursory examination of the second-order relation for the normal stress near the surface indicates that second-order molecular effects could be significant in these experiments.

With respect to experimental techniques, it has been noted that appreciable orifice effects can be present in low-density experiments because of pseudo thermal transpiration effects. An empirical correction due to Knudsen has been applied to these data. A direct measurement of surface pressure, using a transducer with a flush diaphragm, shows that these corrected data can be interpreted as the surface pressure.

## REFERENCES


1. Burnett, D., "The Distribution of Molecular Velocities and the Mean Motion in a Non-Uniform Gas". Proc. London Math. Soc., Vol. 40, p. 382 (1935).

2. Grad, H., "On the Kinetic Theory of Rarefied Gases". Comm. Pure and Appl. Math., Vol. 2, p. 331 (1949).

3. Shen, S.F., "An Estimate of Viscosity Effect on Hypersonic Flow Over an Insulated Wedge". J. Math. Phys., Vol. 31, p. 192 (1952).

4. Pai, S.I., "A Note on Hypersonic Flow Over a Flat Plate". J. Aero. Sci., Vol. 20, No. 7, p. 502 (July 1953).

5. Pai, S.I. and Shen, S.F., "Hypersonic Viscous Flow Over an Inclined Wedge with Heat Transfer". 50 Jahre Grenzschichtforschung, ed. by H. Görtler and W. Tollmien, p. 112 (1955).

6. Cheng, H.K., Hall, J.G., Golian, T.C. and Hertzberg, A., "Boundary-Layer Displacement and Leading-Edge Bluntness Effects in High-Temperature Hypersonic Flow". J. Aero. Sci., Vol. 28, No. 5, p. 353 (May 1961).

7. Hall, J.G. and Golian, T.C., "Shock Tunnel Studies of Hypersonic Flat-Plate Airflows". CAL Report AD-1052-A-10; AFOSR TR 60-142, December 1960.

8. Cheng, H.K., "The Blunt Body Problem in Hypersonic Flow at Low Reynolds Number". IAS Paper 63-92; CAL Report AF-1285-A-10, June 1963.

9. Vidal, R.J. and Wittliff, C.E., "Hypersonic Low-Density Studies of Blunt and Slender Bodies". In Rarefied Gas Dynamics, Vol. II (J.A. Laurmann, Ed.), Academic Press, New York (1963).

10. Hall, J.G. and Hertzberg, A., "Recent Advances in Transient Surface Temperature Thermometry". Jet Propulsion, Vol. 28, No. 11 (November 1958).

11. Vidal, R.J., "Model Instrumentation Techniques for Heat Transfer and Force Measurements in a Hypersonic Shock Tunnel". CAL Report AD-917-A-1, February 1956.

12. Vidal, R.J., "Transient Surface Temperature Measurements". CAL Report 114, May 1962.

13. Knudsen, M., "Thermischer Molekulardruck in Röhren". Annalen der Physik, Vol. 83, p. 797 (1927).

14. Arney, G.D. and Bailey, A.B., "An Investigation of the Equilibrium Pressure Along Unequally Heated Tubes". AEDC-TDR-62-26, February 1962.

15. Arney, G.D. and Bailey, A.B., "Addendum to An Investigation of the Equilibrium Pressure Along Unequally Heated Tubes". AEDC-TDR-62-188, October 1962.

16. Patterson, G.N., Molecular Flow of Gases. Wiley and Sons, New York, 1956.

17. Vidal, R.J., Golian, T.C. and Bartz, J.A., "An Experimental Study of Hypersonic Low-Density Viscous Effects on a Sharp Flat Plate". AIAA Preprint 63-435 (August 1963).

18. Probstein, R.F. and Pan, Y.S., "Rarefied Flow Transition at a Leading Edge". Paper presented at the International Symposium on Fundamental Phenomena in Hypersonic Flow, Buffalo, New York, June 25-26, 1964.

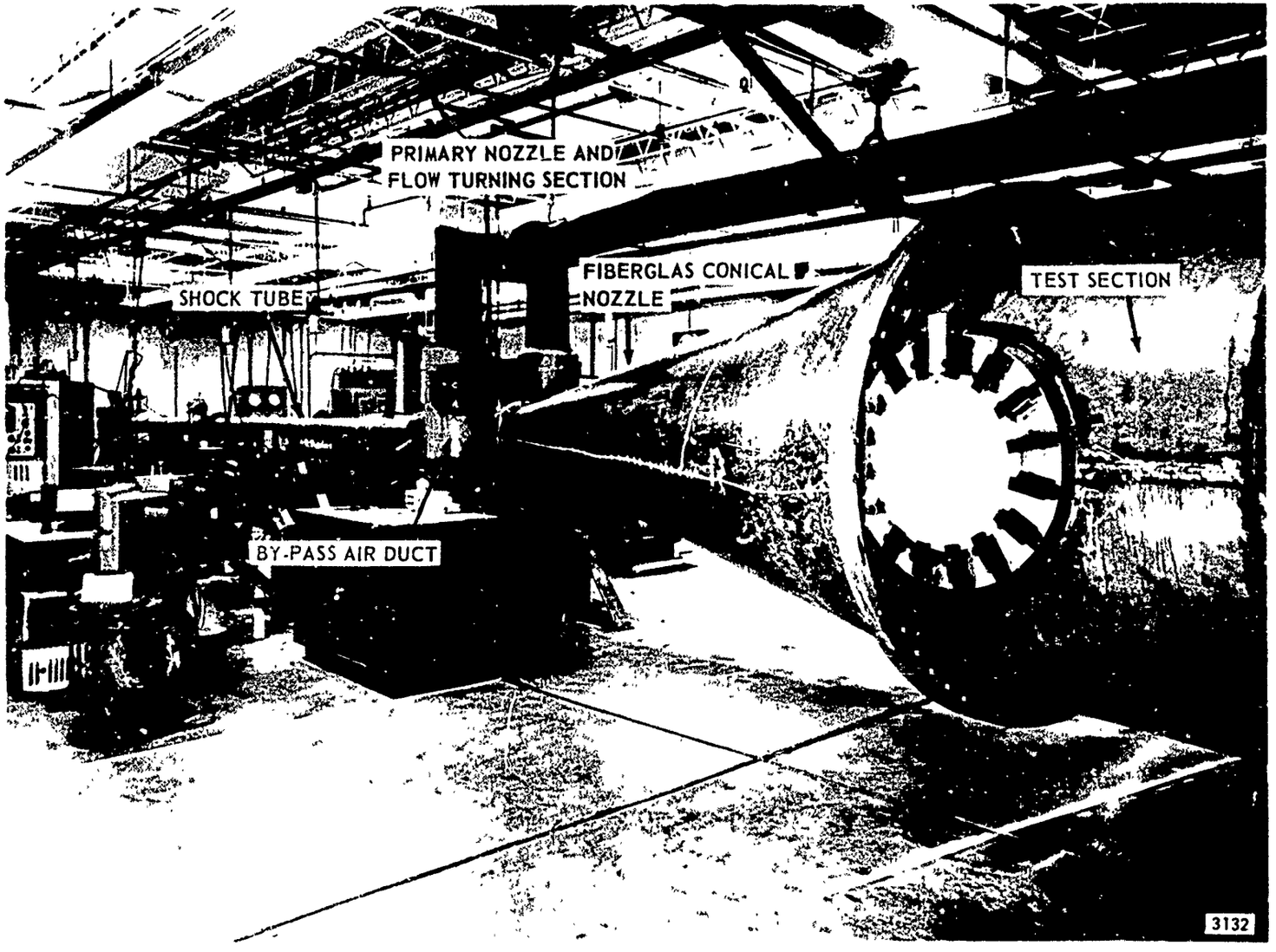


Figure 1 CAL SIX-FOOT HYPERSONIC SHOCK TUNNEL

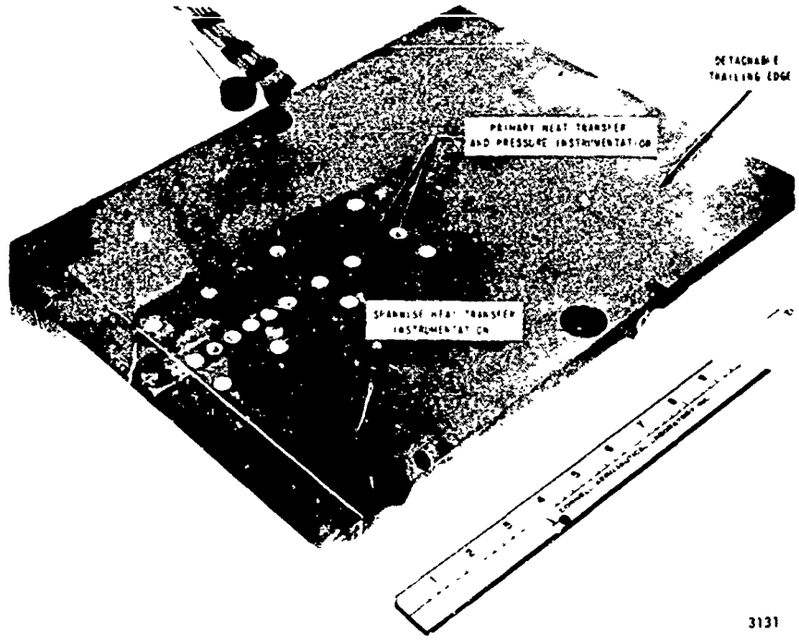


Figure 2a LARGE-SCALE FLAT PLATE MODEL

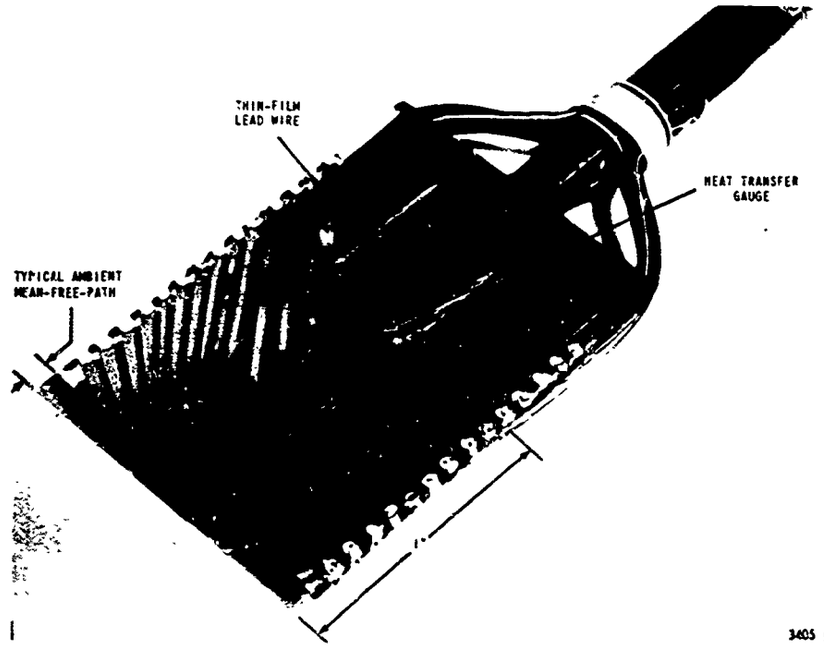


Figure 2b SMALL-SCALE FLAT PLATE MODEL

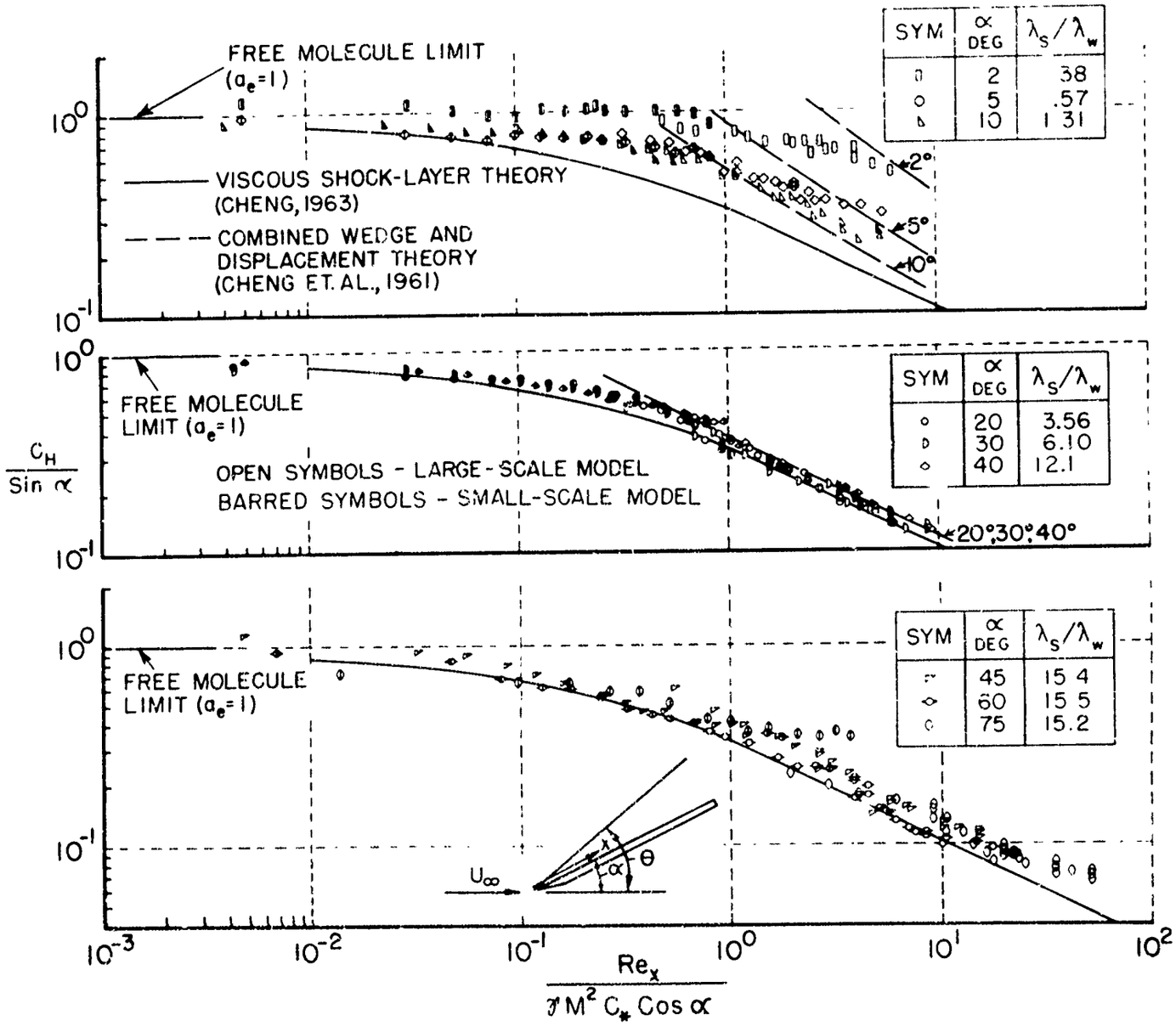


Figure 3 COMPARISON OF EXPERIMENT AND THEORY FOR VISCOUS SHOCK LAYER WEDGE FLOW

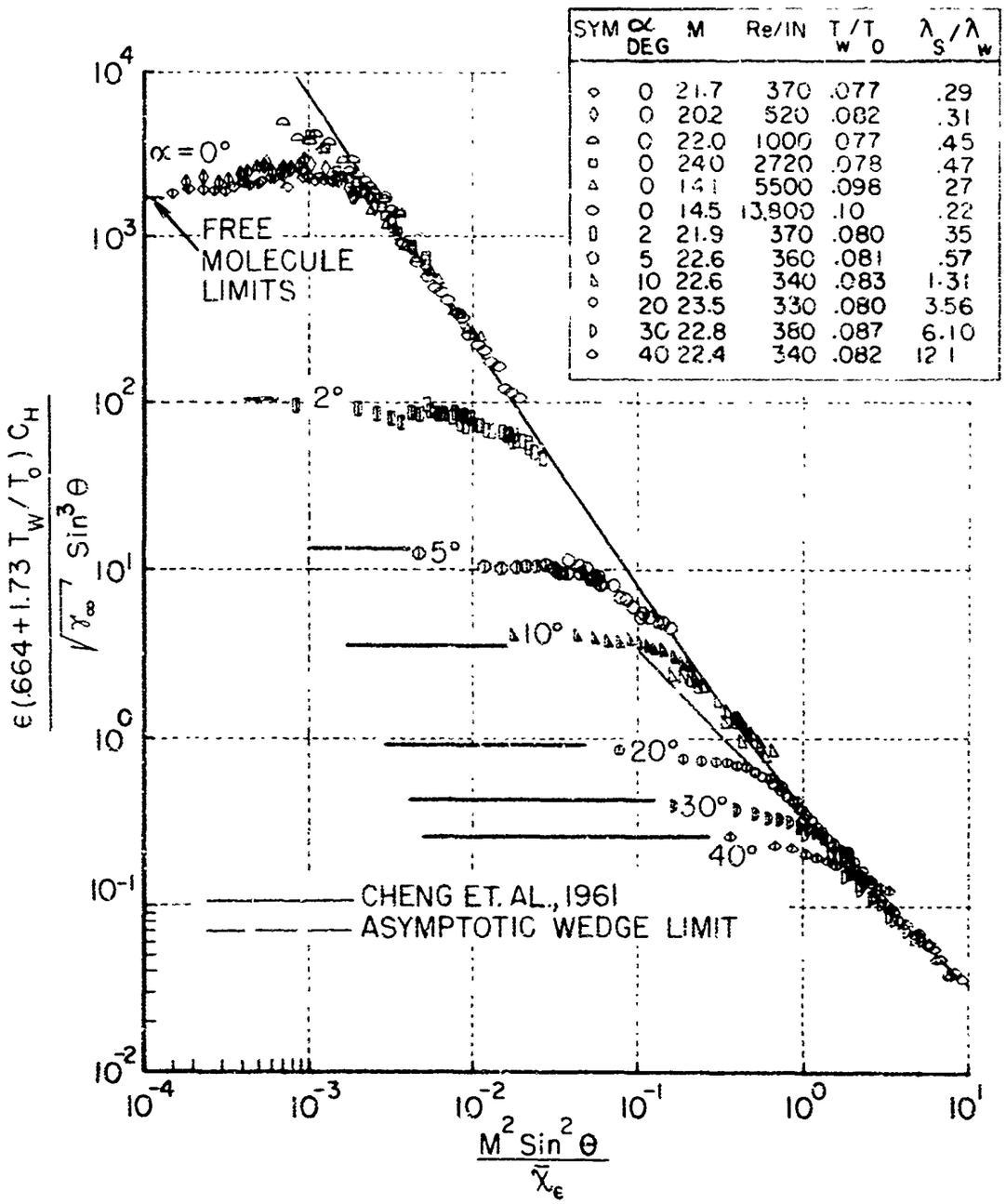


**Figure 4 COMPARISON OF EXPERIMENT AND THEORY FOR COMBINED EFFECTS OF BOUNDARY-LAYER DISPLACEMENT AND WEDGE ANGLE**

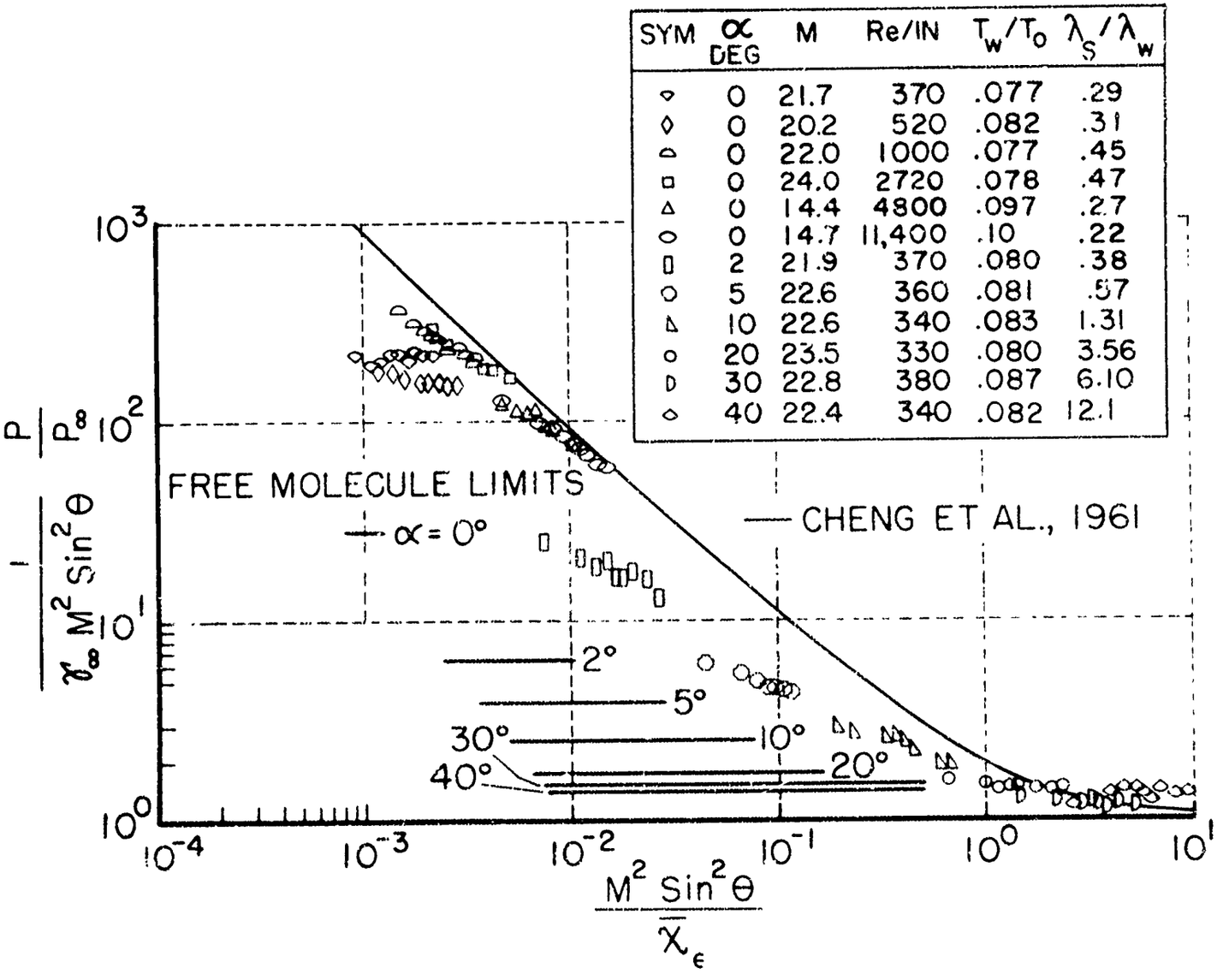


Figure 5 COMPARISON OF EXPERIMENT AND THEORY FOR COMBINED EFFECTS OF BOUNDARY-LAYER DISPLACEMENT AND WEDGE ANGLE